
Article:
Anas Tomeh, M., Hadianamrei, R., Sun, W. et al. (3 more authors) (2021) Stiffness-tuneable nanocarriers for controlled delivery of ASC-J9 into colorectal cancer cells. Journal of Colloid and Interface Science, 594. pp. 513-521. ISSN 0021-9797

https://doi.org/10.1016/j.jcis.2021.03.086

Journal of Colloid and Interface Science 594 (2021) 513–521

Contents lists available at ScienceDirect

Journal of Colloid and Interface Science

journal homepage: www.elsevier.com/locate/jcis

Regular Article

Stiffness-tuneable nanocarriers for controlled delivery of ASC-J9 into colorectal cancer cells

Mhd Anas Tomeh [a], Roja Hadianamrei [a], Weizhen Sun [a], Defeng Xu [b], Stephen Brown [c], Xiubo Zhao [a,b,*]

[a] Department of Chemical and Biological Engineering, University of Sheffield, Sheffield S1 3JD, UK
[b] School of Pharmacy, Changzhou University, Changzhou 213164, China
[c] Department of Biomedical Science, University of Sheffield, Sheffield S1 2TN, UK

GRAPHICAL ABSTRACT

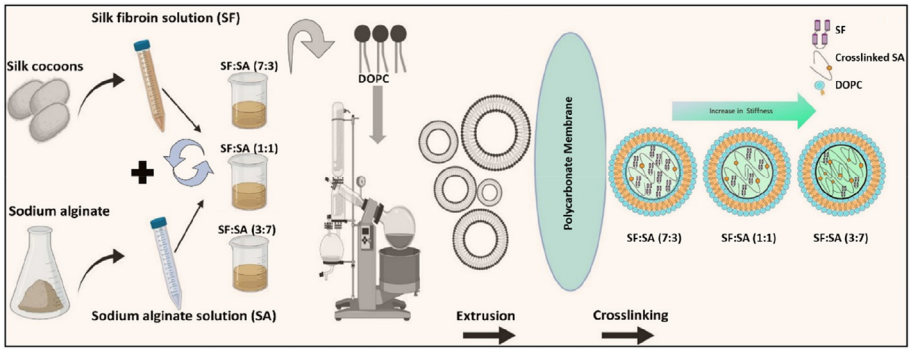

ARTICLE INFO

Article history:
Received 19 January 2021
Revised 2 March 2021
Accepted 14 March 2021
Available online 18 March 2021

Keywords:
Nanocarrier
Silk fibroin
Particle stiffness
Controlled release
Drug delivery
Anticancer
ASC-J9

ABSTRACT

Hypothesis: One of the main challenges in cancer therapy is the poor water solubility of many anticancer drugs which results in low bioavailability at the tumour sites and reduced efficacy. The currently available polymer-based anticancer drug delivery systems often suffer from low encapsulation efficiency, uncontrolled release, and lack of long-term stability. Herein, we report the development of novel stiffness-tuneable core–shell nanocarriers composed of naturally derived polymers silk fibroin (SF) and sodium alginate (SA) inside a liposomal shell for enhanced cellular uptake and controlled release of hydrophobic anticancer agent ASC-J9 (Dimethylcurcumin). It is anticipated that the stiffness of the nanocarriers has a significant effect on their cellular uptake and anticancer efficacy.
Experiments: The nanocarriers were prepared by thin film hydration method followed by extrusion and cross-linking of SA to obtain a uniform size and shape, avoiding harsh processing conditions. The structural transformation of SF in the nanocarriers induced by SA crosslinking was determined using Fourier transform infrared (FTIR) spectroscopy. The size, zeta potential, morphology and stiffness of the nanocarriers were measured using dynamic light scattering (DLS), transmission electron microscopy (TEM) and atomic force microscopy (AFM). Drug loading and release were measured using UV–Vis spectrophotometry. The cellular uptake and anticancer efficacy of the nanocarriers were studied in HCT 116 human colorectal adenocarcinoma cells and 3D tumour spheroids using high content microscopy.
Findings: The synthesized nanocarriers had high encapsulation efficiency (62–78%) and were physically stable for up to 5 months at 4 ℃. The release profile of the drug from the nanocarriers was directed by

* Corresponding author at: Department of Chemical and Biological Engineering, University of Sheffield, Sheffield S1 3JD, UK.
E-mail address: xiubo.zhao@sheffield.ac.uk (X. Zhao).

https://doi.org/10.1016/j.jcis.2021.03.086

their stiffness and was easily tuneable by changing the ratio of SF to SA in the core. Furthermore, the designed nanocarriers improved the cellular uptake and anticancer activity of ASC-J9, and enhanced its tumour penetration in HCT 116 3D colorectal cancer spheroids. These findings suggest that the designed core–shell nanocarriers can be used as a highly efficient drug delivery system for cancer therapy.

1. Introduction

One of the main obstacles to overcome in cancer therapy is designing non-toxic and biodegradable carriers for safe and efficient anticancer drug delivery. Recent advances in nanotechnology and polymer engineering have opened doors to new and more efficient approaches to cancer therapy using nano-formulations [1–3]. However, the inherent low solubility of many anticancer agents in water and biological fluids complicates their formulation process and hinders their clinical applications [4–6]. Moreover, low local concentration of these drugs in the tumour tissue due to insufficient diffusion and/or short elimination half-life ($t_{1/2}$) may result in multidrug resistance (MDR) which is one of the major challenges in cancer treatment especially in the case of metastatic cancers such as breast and colon cancers [7–10]. For example, $t_{1/2}$ of the hydrophobic anticancer agent ASC-J9 was found to be less than 6 h following an intravenous injection in mouse, which reduces the bioactivity in certain tissues [11]. Increasing the exposure time of ASC-J9 to the cancer cells reduces the half maximal inhibitory concentration (IC_{50}) values due to the cumulative cytotoxic effect [12]. Therefore, the development of novel drug delivery systems (DDSs) for efficient loading, enhanced aqueous solubility, and improved cellular uptake of hydrophobic anticancer agents within the elimination time window has received more attention over the past decade [13–15].

In order to design effective nano-carriers, several factors must be taken into consideration such as size, geometric shape, elasticity, and surface charge [16–20]. Recently, nanoformulations, such as liposomes / lipid nanoparticles [21,22], micelles [19], polymer conjugates, and polymeric nanoparticles [14], have been prepared to function as vectors for many hydrophobic anticancer agents showing great potential for delivering these agents to the target cells [15,23]. Although engineered nanoparticles with optimized size and shape can improve drug delivery, they still lack efficient targeting and their accumulation in the tumour tissue is limited to less than 1% [24]. Other limitations of the conventional nanocarriers include low encapsulation efficiency (EE), uncontrolled release, "initial burst effect" (rapid release of the loaded drug within the first few minutes) and lack of long-term stability [19,25,26]. Most of the currently available literature has focused on improving the properties of the nanoparticles and nanoliposomes through modifying their surface or their outer shell respectively [22,27] and only few recent studies have investigated the impact of modifying the physical characteristics of the particle core on their properties such as EE, release profile, and cellular uptake. In the present work, we present novel nanocarriers with tuneable physical properties through incorporation of a combination of silk fibroin (SF) and sodium alginate (SA) cores in the liposomal shells. Unlike the previous studies, the focus is on modification of the physical properties of the core in order to enhance the EE, improve the cellular uptake and achieve controlled drug release.

SF obtained from cocoons of *bombyx mori* silkworm is an FDA approved naturally derived biopolymer which exhibits unique features such as biocompatibility, biodegradability, and the ability to enhance the stability of the loaded drug [28–30]. SF can undergo diverse structural transformations at the molecular level. The most studied transformation is the shift in the ratio of α-helix to β-sheet [31]. This transformation results in insolubilizing SF to form micro and nanoformulations that can be employed for drug and gene delivery [28]. Furthermore, SF can be easily processed by various techniques to prepare a variety of micro and nanostructures including sponges, microspheres, nanogels, and nanoparticles for biomedical applications [32]. The physical properties of silk can be improved by blending it with other polymers. A recent study by De Moraes et *al.* [33] has reported modified physical characteristics of SF when blended with polysaccharides such as SA [33]. SF/SA blends have almost no toxicity, high miscibility, less heterogenicity and restricted phase separation due to the interaction between SA carboxyl groups and SF amino groups [33]. Furthermore, mixing SA with SF allows SF to shift to β-sheet predominant form (Silk II) which can provide a platform for loading poorly water-soluble compounds through hydrophobic interactions [28,33]. Therefore, the combination of SF and SA has been selected in this study to form the core of the nanocarriers. This combination of polymers also allows for controlling the elasticity of the nanocarriers.

Particle elasticity hypothesis has drawn increasing attention in the field of nanomedicine in the past few years [34]. Modifying the rigidity of the nanoparticles can alter their cellular uptake pathways (e.g. fusion and/or endocytosis), as well as other properties such as EE and drug release [20,35–37]. For example, Sun et *al.* [36] developed modified PLGA-lipid nanoparticles with different rigidity by altering the injection order of PLGA and PEG-lipid solutions in the microfluidic system to vary the amounts of water in between the polymeric core and the lipid shell [36]. However, this method employed synthetic polymers and organic solvents which is not desirable for biomedical applications. In a more recent study conducted by Guo et *al.* [35] the elasticity of the crosslinked nanogel cores was altered by changing the crosslinker concentration [35]. In the present study, nanocarriers consisting of a lipid shell and a core composed of a combination of SF and SA have been developed using a simple procedure that does not require any organic solvents, synthetic polymers or high concentrations of the crosslinkers, and used for delivery of highly hydrophobic anticancer agent ASC-J9 to HCT 116 colorectal adenocarcinoma cells. ASC-J9 has been used for the treatment of different types of cancer including prostate cancer and breast cancer due to its ability to enhance the degradation of androgen receptors (AR) and increase the downstream apoptotic markers [12,14]. However, there are no reports of the use of ASC-J9 for the treatment of colorectal cancer. The stiffness of the designed nanocarriers was simply tuned by changing the ratio between SF and SA. To the best of our knowledge, using the combination of SF and SA for tuning the stiffness of the nanocarriers, regulating their cellular uptake and drug release has not been reported elsewhere.

2. Materials and methods

2.1. Materials

Bombyx mori silk was obtained from Jiangsu, P.R. China. Sodium carbonate (99% pure) was purchased from Alfa Aesar. 1,2-dioleoyl-*sn-glycero*-3-phosphocholine (DOPC, 99% pure) was purchased from Avanti Polar Lipids, US. Dimethylcurcumin (ASC-J9, 98% pure) was provided by Changzhou University, China. Sodium alginate

($C_6H_9NaO_7$, 99% pure), sodium salicylate ($C_7H_5NaO_3$, 99% pure), calcium chloride ($CaCl_2$, 93% pure) and foetal bovine serum (FBS) were purchased from SIGMA-ALDRICH, Gillingham, UK. DMEM (Dulbecco's Modified Eagle Medium) and Hoechst 33,342 (99% pure) were purchased from Thermo Fisher Scientific. Flash Phalloidin™ 594 was purchased from Biolegend.

2.2. Preparation of SF and SA solutions

To extract the SF, the silk cocoons were boiled in 0.02 M sodium carbonate solution for 30 min and rinsed in DI water to remove any traces of the dissolved sericin. After drying, the degummed fibres of SF were dissolved in Ajisawa's reagent ($CaCl_2$/ ethanol/ water = 1: 2: 8 M ratio) at 80 °C for 90 min followed by dialysis in a cellulose tube (FLOAT-A-LYZER G2 dialysis tubing MWCO 12 kDa, Spectrum Labs, Rancho Dominguez, CA, USA) against DI water for 2 days to remove $CaCl_2$ and ethanol. The solution was then centrifuged at 12,000 rpm and filtered through a 0.45 μm filter. The SA solution was prepared by dissolving SA powder in DI water (20 mg/mL) at 30 °C and kept on constant stirring overnight.

2.3. Synthesis and characterization of the SF/SA incorporated nanocarriers

DOPC (10 mg) was dissolved in chloroform (1 mL) in a round bottom flask. The solvent was evaporated using a rotary evaporator to form a thin layer of lipid which was then hydrated with 1 mL of SF/SA mixture (with different ratios for each formulation) at 35 °C for 10–15 min to form multilamellar lipo-gel vesicles (MLV). Unencapsulated SF/SA was removed using 30 k Amicon Ultra Centrifugal Filters at 5,000 rpm for 15 min. MLVs were extruded through a 200 nm polycarbonate membrane (Avanti Mini-Extruder) 8 times to form small uniform nanocarriers.

2.4. Preparation of ASC-J9 loaded nanocarriers

Three formulations of nanocarriers containing different ratios of the biopolymers (SF:SA 7:3, 1:1, 3:7) were prepared and loaded with the hydrophobic anticancer drug ASC-J9. The drug loading and crosslinking of the SA monomers within the biopolymeric core were performed simultaneously by adding ASC-J9 and $CaCl_2$ (10 mM) dropwise to the nanocarrier solutions (1:1, v:v). After 1 h incubation with constant stirring at 30 °C, the crossed-linked nanocarriers were dialyzed in FLOAT-A-LYZER G2 dialysis tubing (MWCO 1000 kDa) in PBS for 8 h at 4 °C to remove the remaining $CaCl_2$.

2.5. Encapsulation efficiency measurement

To measure the EE, the unencapsulated drug was removed by gel filtration using Sephadex G50 in an HR 10/30 column with DI water as eluent at a flow rate of 1 mL/min. Next, 50 μL of the sample was diluted with DMSO in an eppendorf tube and vortexed for 1 min. The encapsulated drug was quantified by UV–Vis spectrophotometry (JENWAY 6715, Bibby Scientific, UK) at 435 nm using standard calibration curves for ASC-J9 in DMSO and PBS. Each sample was assayed in triplicate. The EE% was determined by Equation (1):

$$EE\% = \frac{Encapsulated\ ASC-J9}{Initally\ added\ ASC-J9} \times 100\% \quad (1)$$

2.6. Nanocarrier characterization

2.6.1. Particle size and zeta potential measurement

The size and Zeta potential of the different formulated nanocarriers were measured in PBS (pH 7.4) using dynamic light scattering (DLS) (NanoBrook 90 plus Pals Particle size Analyzer, Brookhaven Instrument, NY, USA). The temperature was set at 20 °C and the diode laser with a wavelength of 660 nm was used.

2.6.2. Fourier transform infrared spectroscopy

Fourier transform infrared (FTIR) spectroscopy (IR Prestige-21, Shimadzu, UK) was used to investigate the chemical interaction between SF and SA and to detect the SF structural transformations. Nanocarrier formulations were mixed with 1% triton X-100 to disturb the lipid shell and then centrifuged using 30 k Amicon Ultra Centrifugal Filters at 10,000 rpm to remove the remaining lipid. The samples were allowed to air dry on the diamond attenuated total reflectance (ATR) attachment (ATR apparatus, Pike Technologies, USA) of the spectrophotometer. The range of wave numbers was set from 500 to 3000 cm^{-1} and the spectrum was read using the Happ-Genzel apodisation function over 64 scans with a resolution of 4 cm^{-1}. The region (1575–1750 cm^{-1}) which is assigned to amide I was investigated to determine the secondary structural changes of SF.

2.6.3. Atomic force microscopy

To obtain the core size and the morphology of the nanocarriers, Atomic Force Microscopy (AFM) (Dimension Icon with ScanAsyst, Bruker Corporation, U.S.A) was used. Particle solutions were dropped on mica substrates and dried with gentle airflow before placing them on the sample stage, SCANASYST-AIR tips were used to perform the analysis in dry mode. For the young's modulus measurement, the nanocarriers were analysed in liquid mode using FASTSCAN-D with a 5 nm tip radius. The force-distance curves obtained from the instruments were used to calculate young's modulus using Hertz model (Eq. (2)).

$$F = \frac{4}{3}\frac{E}{(1-\nu^2)}\sqrt{R\delta^{3/2}} \quad (2)$$

where F is the force from force curves, E is Young's modulus, ν is Poisson's ratio, R is the radius of the indenter tip, and δ is the indentation depth. The extracted data were analysed with NanoScope Analysis 1.9 software.

2.6.4. Transmission electron microscopy

Transmission electron microscopy (TEM) images were obtained using an FEI Tecnai BioTWIN G2 sprint. The accelerating voltage was set to 80 Kv. 10 μL of the nanocarrier solution was deposited onto carbon-coated copper grids for 1 min and blotted with a filter paper. The grids were then left to dry at 25 °C and stained with 0.1% (w/v) phosphotungstic acid for 1 min and then blotted again with a filter paper. Finally, the samples were washed with DI water and kept for measurement at room temperature. Images were recorded using a Gatan Orius SC1000B bottom-mounted digital camera and Gatan Digital Micrograph software.

2.7. Storage stability

The prepared nanocarriers were stored in a dark place at 4 °C for 6 months and their physical stability was monitored by measuring the changes in particle size during the storage period.

2.8. In vitro drug release

The *in vitro* drug release profile of the ASC-J9 loaded nanocarrier solutions was determined by transferring aliquots of ASC-J9 nanocarrier solution (63 μM) into FLOAT-A-LYZER G2 dialysis tubing (MWCO 1000 kDa). The tubes were dialyzed against 50 mL sodium salicylate solution (1 M) at 37 °C with rotation at 150 rpm. The concentration of ASC-J9 released at various time

points was measured by UV–Vis spectrophotometry at 435 nm. The drug release profile of the ASC-J9 solution was determined under identical conditions for comparison. The experiments were performed in triplicate and the values were reported as mean ± SE.

2.9. Cellular uptake

The cellular uptake studies were carried out using HCT 116 human colorectal adenocarcinoma cells. The cells were cultured in DMEM supplemented with 10% FBS and 1% penicillin/streptomycin in 37 ℃ and under 5% CO_2. For the cellular uptake experiments, the HCT 116 cells were cultured in 96 well plates at a seeding density of 4×10^3 cells per well and were incubated for 24 h. Then the cells were treated with the drug solution or the drug-loaded nanocarriers and incubated for 6 h at which point the media was replaced with fresh media. The experiments were carried out in two different conditions. The first set of experiments were performed in the cells growing in DMEM supplemented with 10% FBS. In the second set of experiments, the cells were starved in serum-free media for 4 h prior to the addition of the drug solution or drug-loaded nanocarriers and then the media were replaced with media supplemented with 10% FBS. At designated time points, the cells were fixed with 3.7% formaldehyde, stained with Hoechst 33,342 and Flash Phalloidin™ 594 and imaged with a high content fluorescent automated widefield microscope (ImageXpress® Micro System). The images were analysed using MetaXpress® software 5.3.01 (Molecular Devices). Two algorithms were used to determine the cellular uptake: one for quantifying the drug or drug-loaded objects within the cell, and one for measuring the average integrated intensity of the drug within the cytosol.

2.10. Uptake in 3D spheroids

The 3D spheroids were prepared by growing HCT 116 cells in ultra-low attachment 96 well plates at a seeding density of 8×10^3 cells per well for 48 h. The spheroids were treated with 25 μM ASC-J9 solution or ASC-J9 loaded nanocarriers for 12 h and then fixed with 3.7% formaldehyde and stained with Hoechst 33,342 and imaged with the high content microscope.

2.11. Statistical analysis

The statistical analysis of the data was carried out using GraphPad Prism 7.04. The Student's *t*-test was used for comparison between two groups, and the one-way ANOVA was used for the comparison between multiple groups. All experiments were performed in triplicate and the data were presented as the mean ± standard error of three repeats unless otherwise mentioned. Statistical significance was considered when the p value was less than 0.05.

3. Results & discussion

Due to its strong activity towards cancer cells, curcumin has been one of the most studied natural compounds for cancer therapy [30]. Recently, curcumin analogues with higher anticancer efficacy such as ASC-J9 have been developed through structural modifications such as methylation [30,31]. Nonetheless, these structural changes have led to a tangible increase in the hydrophobicity of the resulting drug molecules [32]. ASC-J9 increases the downstream apoptotic markers to a higher extent compared to curcumin, which results in enhanced anticancer activity [7]. On the other hand, ASC-J9 is more hydrophobic than curcumin and has a relatively short elimination time ($t_{1/2}$ < 6 h) which limits its anticancer activity in the tumour tissue [6]. Recently, ASC-J9 was formulated with polymeric nanoparticles (PLGA) to improve its circulation time and control the drug release [14]. However, these polymeric formulations do not provide stiffness tunability and their impact on cellular uptake within the drug elimination time was not assessed. The present work was aimed at developing nanocarriers with tuneable properties for enhanced loading, improved aqueous solubility and enhanced cellular uptake of ASC-J9 before it is cleared from the body.

3.1. Physical characterization of the ASC-J9 nanocarriers

The designed nanocarriers consist of a lipid bilayer shell and a biopolymeric core which serves as vector for ASC-J9. Crosslinking SA with calcium ions within the core transforms the core into a hydrogel. The rigidity of the resulting hydrogel core is modulated by blending SA with SF which alters the amount of the SA monomers required to make the hydrogel network (Fig. 1.A). The DOPC lipid shell provides a template for controlling the overall size of the nanocarriers via the extrusion method [33]. This shell maintains the size of the nanocarrier in the aqueous phase as shown in Fig. 2.A. The DLS characterization showed a similar hydrodynamic diameter of ~170 nm for all three formulations. The zeta potential was slightly negative in the nanocarrier formulation SF:SA (3:7). However, the zeta potential became more negative when the ratio of SF to SA was increased in the nanocarrier formulation (Fig. 2.C). Zwitterionic lipids shell (e.g. DOPC) entrapping SA hydrogel has shown slightly negative zeta potential (−4 to −10 mv) [35]. On the other hand, SF is a negatively charged protein in its β-sheet form (−29 to −43) mv [38] and therefore increasing the ratio of SF to SA allows more SF molecules to incorporate in the lipid shell which can explain the reduction in the absolute value of zeta potential of the SF:SA (7:3). The three nanocarrier formulations demonstrated size stability for up to 5 months when stored at 4 °C (Fig. 2.F). After 6 months, significant variation in the size of the nanocarriers was observed in the SF:SA (7:3) formulation which is suspected to be due to aggregation.

The nanocarrier cores were made of multiphase blends of SF and SA which can exhibit different morphological states. Typically, dispersing one polymer in the matrix of another induces changes in the properties of the mixture, and these changes are mainly controlled by the matrix properties [34]. TEM and AFM were used to provide a clearer insight into the interior structure of the nanocarriers. As shown in Fig. 1, spherical nanocarriers were formed in the three formulations. The dense hydrogel core appears darker than the lipid bilayer in the TEM image (Fig. 1.B). The AFM scanning was carried out to determine the morphology of the nanocarriers. The stiffness of the core correlates to the ratio of SA to SF in the nanocarrier formulation. The AFM scans revealed that the formulation with the high SF to SA ratio (low stiffness) has an increase in the core size in comparison to the formulation with the low SF to SA ratio when scanned in the dry mode (Fig. 1.C & Fig. 2.B). This can be explained by higher core deformation during scanning due to less SA hydrogel network which maintains the structure of the core. The high percentage of SA in the core can form more hydrogel network after adding the crosslinker, making the nanocarrier more rigid and less deformable. Different amount of interfacial water entrapped during the preparation and hydrophobic interaction between the two polymers can also play a role in modifying the deformability of the nanocarriers [39]. The height profiles obtained by AFM show an increase in the surface roughness of the core structure by increasing the SF to SA ratio (Fig. 1.E). On the other hand, high SA content provides a smooth core surface because of forming a tighter hydrogel network. The Young's modulus was measured using AFM in liquid mode (Fig. 2.G). The Young's modulus decreases with the increasing SF:SA ratio, indicating the presence of SF reduced the stiffness of the nanocarriers,

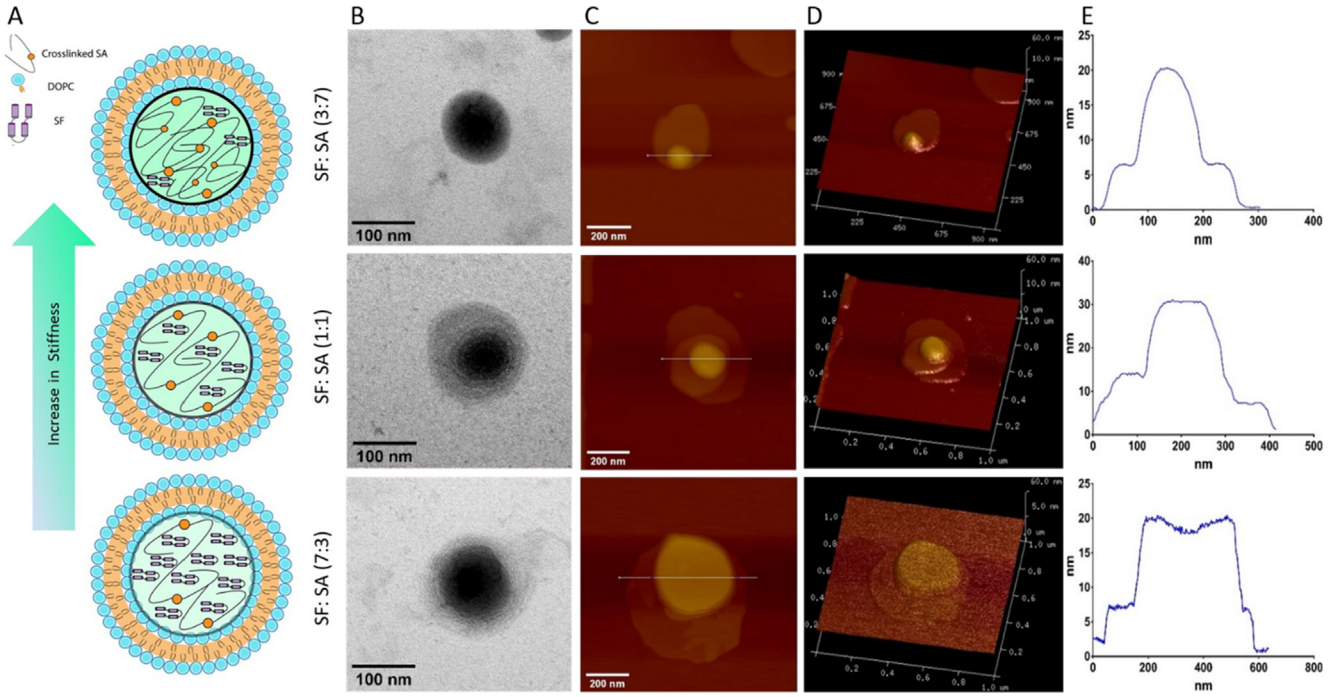

Fig. 1. (**A**) Schematic representation of the three types of synthesized nanocarriers, entrapping silk fibroin (SF) and sodium alginate (SA) cores (at different SF/SA ratios) in the lipid shells. (**B**) TEM images of the synthesized nanocarriers. (**C**) AFM images of the nanocarriers showing the polymeric core and the lipid shell in dry mode. (**D**) 3D AFM images of the nanocarriers. (**E**) Hight profiles of the nanocarriers obtained by AFM.

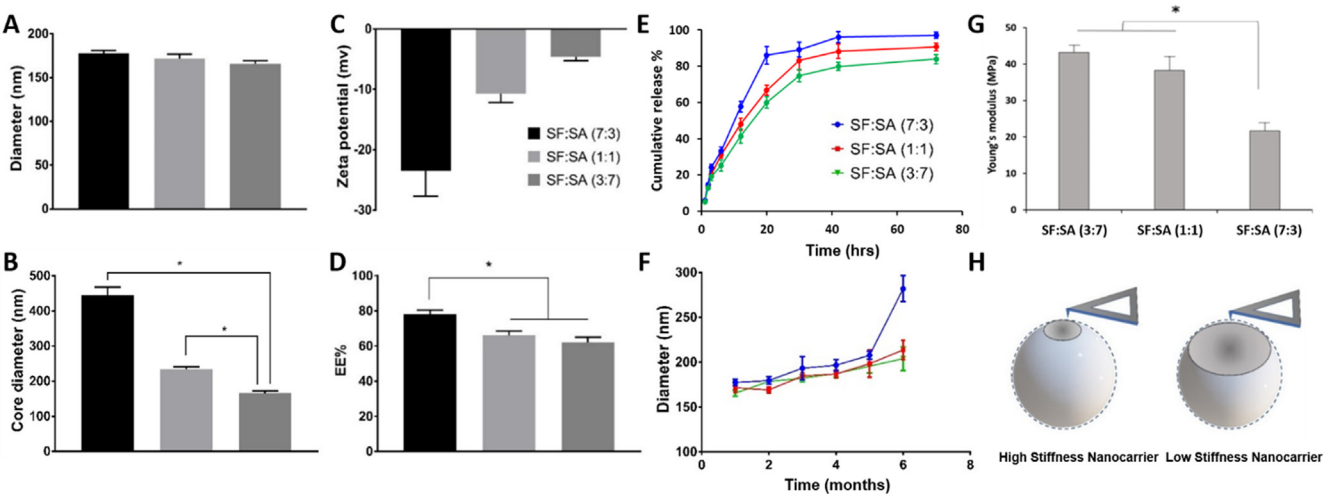

Fig. 2. Characterization of the synthesized nanocarrier formulations with varying properties. (**A**) Particle size of the nanocarriers measured by dynamic light scattering (DLS). (**B**) Core size of the nanocarriers obtained by AFM scans in dry mode. (**C**) Zeta potential of the nanocarriers measured by DLS. (**D**) Encapsulation efficiency (EE) of ASC-J9 in different nanocarrier formulations. (**E**) Release profiles of ASC-J9 encapsulated in different nanocarrier formulations. (**F**) Changes to the diameters of nanocarriers over 6 months measured by DLS. (**G**) The Young's moduli of the nanocarriers characterized in liquid mode by AFM. (**H**) Schematic illustration of high and low stiffness nanocarriers during Young's moduli measurements in AFM. * Denotes values of $P < 0.05$.

which had an implication in drug loading and release subsequently.

FTIR spectroscopy has been a useful technique to investigate the transformation of SF to β-sheet structure. The main absorption peaks for unprocessed SF and SF blends in the nanocarrier formulations are presented in Fig. 3 and Table 1. The FTIR spectrum of unprocessed SF shows the absorption bands assigned to amide I (1616.2 cm^{-1}) and II (1508.2 cm^{-1}) that correspond to β-sheet predominant conformation (silk II) [27]. Amide III absorption band (1228.5 cm^{-1}) corresponds to silk I conformation with α-helix predominance. The nanocarrier formulations containing blends of SF and SA (7:3, 1:1 & 3:7) present spectra similar to the unprocessed SF with additional absorption bands that are assigned to the C═O, O—H, and C—O stretching in the SA structure [27,35]. SF amide I and III absorption bands are overlapping with structural groups of SA; therefore, the amide II band was used to analyse the spectra and detect the transformation to silk II. As illustrated in Fig. 3, the amide II band clearly shifted to a higher wavelength and was detected at 1528.2 cm^{-1} indicating silk II conformation.

3.2. ASC-J9 encapsulation and release

Drug encapsulation efficiency is one of the most important features for determining the effectiveness of the designed delivery

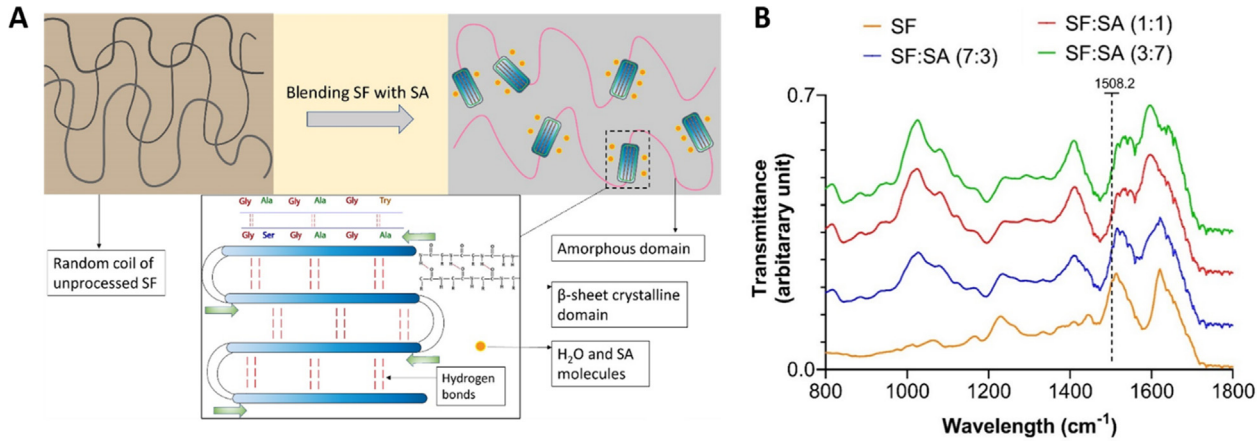

Fig. 3. (**A**) Schematic representation of silk fibroin (SF) structural transforamtion in the designed nanocarries as a result of blending with sodium alginate (SA). (**B**) FTIR spectra of SF and SF/SA blends with different ratio in the nanocarrier core.

Table 1
FTIR absorption peaks of silk fibroin (SF), sodium alginate (SA), and SF/SA mixture.

100% SF	SF/SA mixture	100% SA	Attribution of absorption peaks
–	1731.9	1731.9	C=O stretching
1620.1	1622.0	1635.5	Amide I and antisymmetric = COO = stretching overlap
1505.2	1522.0	–	Amide II
1228.5	1236.2	1238.2	Amide III and C=O stretching overlap
–	1080.0	1076.2	O—H bending
–	1029.9	1027.9	O—H bending
–	927.7	927.7	C—O vibration

system as a drug carrier especially in nanoformulations [20]. For efficient entrapment of ASC-J9 in the polymeric core matrix, the drug and the crosslinking agent ($CaCl_2$) were added simultaneously. The drug molecule enters the matrix with calcium ions that are transforming the structure of SA to form the hydrogel network. Changing the nature of the core from liquid state to polysaccharide hydrogel during crosslinking can restrict the Brownian motion of the ASC-J9 molecules and enhance their retention in the nanocarrier. A previous study has shown a significant increase in encapsulation efficiency as a result of hydrogel network formation. However, no significant change in EEs was observed in different hydrogel stiffness when one polymer was used [28]. In the current study, two polymers (SF & SA) have been used and the interaction between the two during crosslinking allows SF to transform to β sheet providing a platform for hydrophobic interaction with ASC-J9 molecules. This can explain the higher EE observed in high SF content nanocarrier formulation (SF:SA 7:3) in comparison to the formulation with lower SF content (SF:SA 1:1, 3:7) (Fig. 2.D).

The effect of modifying the nanocarrier stiffness on the drug release kinetics was also investigated. The nanocarrier formulation with higher stiffness (higher modulus) exhibited slower drug release (Fig. 2.E). The high percentage of SA results in a tighter hydrogel network and smaller pore size (Fig. 1.D&E) which consequently results in higher retention and slower release of the encapsulated drug (Fig. 2. D). These results suggest enhanced EE and tunable drug release achieved by modification of the nanocarrier core composition.

3.3. In vitro cellular uptake study

The designed nanocarriers consist of a combination of biopolymers that are individually approved by the FDA for pharmaceutical applications and regarded as biocompatible, nonimmunogenic, and nontoxic polymers [28,40]. To confirm the lack of toxicity of the unloaded nanocarrier formulations, the cell population was evaluated after treatment with unloaded nanocarriers (SF:SA 7:3, 1:1 & 3:7) (Fig. 5.D). The reduction in the cell population ranged between 1 and 11% indicating very low toxicity.

To investigate the internalization of the nanocarriers and their payload release in HCT 116 colorectal adenocarcinoma cells, the cells were treated with ASC-J9 (25 μM) or ASC-J9 loaded nanocarriers for 6 h to simulate the drug availability time *in vivo* before elimination. The experiments were carried out in two conditions (10% FBS & 0% FBS) to mimic different *in vivo* physiological conditions. The treatments were removed after 6 h by replacing the media to ensure that the intensity measurements are assigned only to the uptaken drug. Like curcumin, the ASC-J9 molecule is autofluorescent ((λ_{exc} = 420 nm; λ_{emi} = 522 nm) and this property has been used previously for cell tracking and measuring cellular uptake [14,15,41]. The enhanced cellular uptake by HCT 116 cells is evident from the high content images presented in Fig. 4. A weaker fluorescent signal was observed in cells treated with unprocessed ASC-J9 in comparison to ASC-J9 loaded nanocarriers. As it could be observed in Fig. 5 the relative uptake of the ASC-J9 was significantly enhanced when it was loaded into the different nanocarrier formulations. Moreover, the ASC-J9-loaded nanocarriers remained in the cells for up to 72 h after internalization serving as a reservoir for the drug and providing sustained drug release whereas the amount of free ASC-J9 within the cells showed a reduction after 72 h. This is supposed to be due to cellular efflux mediated by transporters such as P-glycoprotein [9].

The anticancer activity of the drug was assessed by measuring the percentage of cells within a population that survived after treatment with the free drug and the drug-loaded nanocarriers at different time points (Fig. 5.C). The free ASC-J9 showed higher activity at 12 h than the drug-loaded into the nanocarriers, causing a 50–60% reduction in the number of cancer cells. However, due to the low concentration of the drug within the cells resulting from lower cellular uptake compared to the drug-loaded nanocarriers, the cells recovered from the drug treatment and restarted growing after 24 h. In the case of drug-loaded nanocarriers, the antiproliferative activity started more slowly but was maintained over a longer period of time (72 h) resulting in a considerable reduction in the cell population (Fig. 5.C). A variation in the anticancer activity was observed among the three nanocarrier formulations at 12 h especially in the absence of FBS. However, all nanocarriers formulations showed a similar pattern after 24 h. This behaviour can be explained by the different drug release trend exerted by different formulations. Overall, it can be conferred from these data that

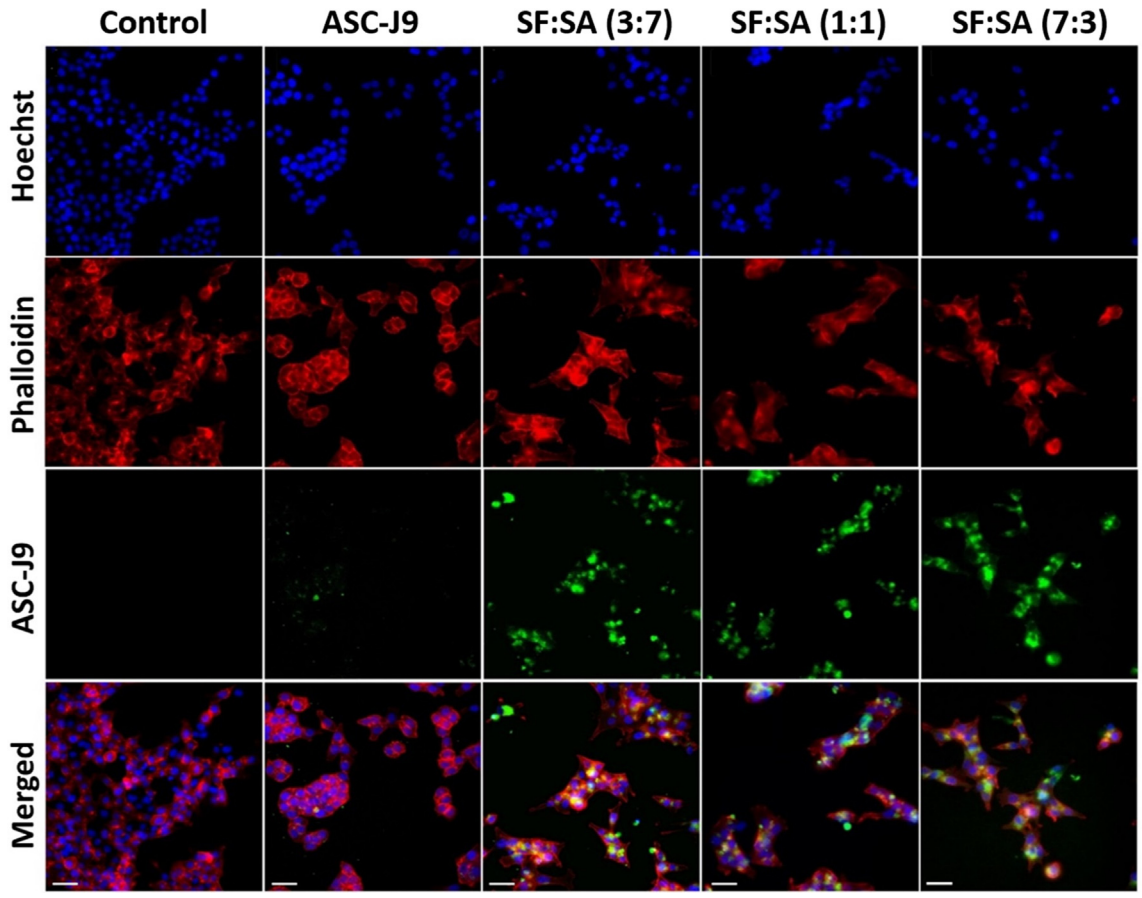

Fig. 4. High content fluorescent microscope images of HCT 116 showing cellular uptake of the free ASC-J9 and different ASC-J9 loaded nanocarriers (SF:SA = 7:3, 1:1, & 3:7) after 24 h (×20 magnification, the scale bar represents 40 μm).

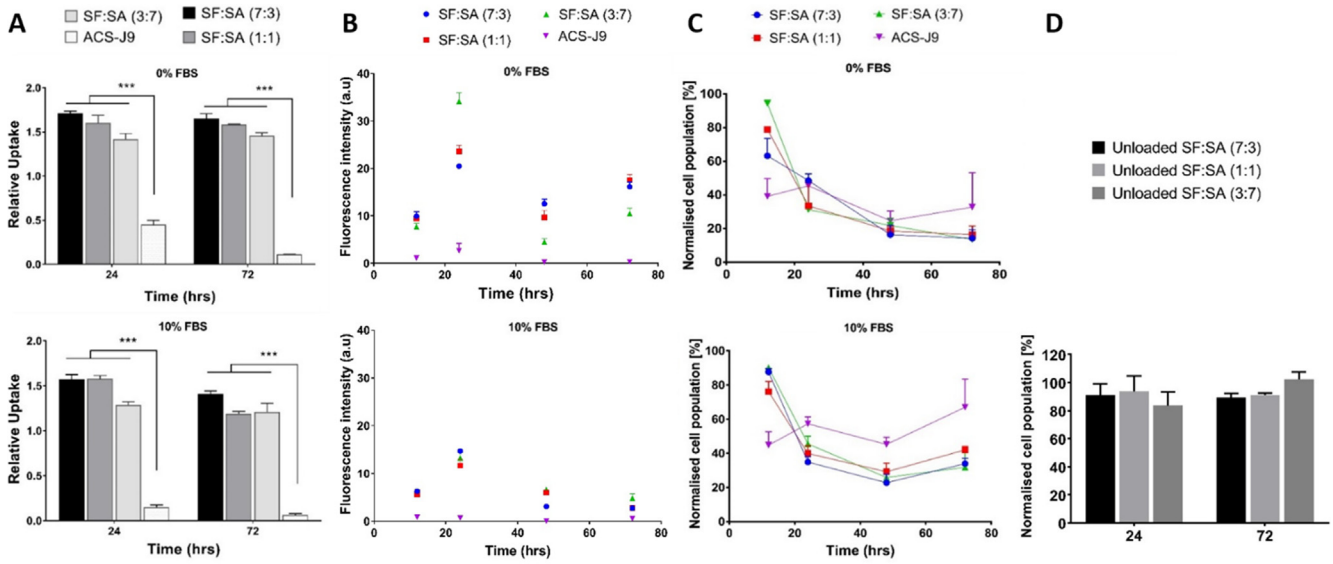

Fig. 5. (**A**) Relative cellular uptake of ASC-J9 loaded nanocarriers formulations and unformulated ASC-J9. (**B**) Fluorescence integrated intensity of ASC-J9 at multiple time points in unformulated form and in nanocarriers form. (**C**) The percentage of survived cells after ASC-J9 and ASC-J9 loaded nanocarriers treatments at multiple time points. (**D**) The effect of the unloaded nanocarrier formulations to the cell population. An asterisk denotes statistical significance as follows: *P < 0.05, **P < 0.01, ***P < 0.001.

the anticancer activity of the ASC-J9 in HCT 116 cells was enhanced by loading into the designed nanocarriers and that the sustained release of the drug from the nanocarriers resulted in a prolonged antiproliferative activity which prevented the cells from recovering.

3.4. Uptake in 3D tumour spheroids

3D tumour spheroids were used as a mimic of the tumours in order to provide a better insight into the drug interaction with the tumour cells as they provide a closer simulation of the tumour

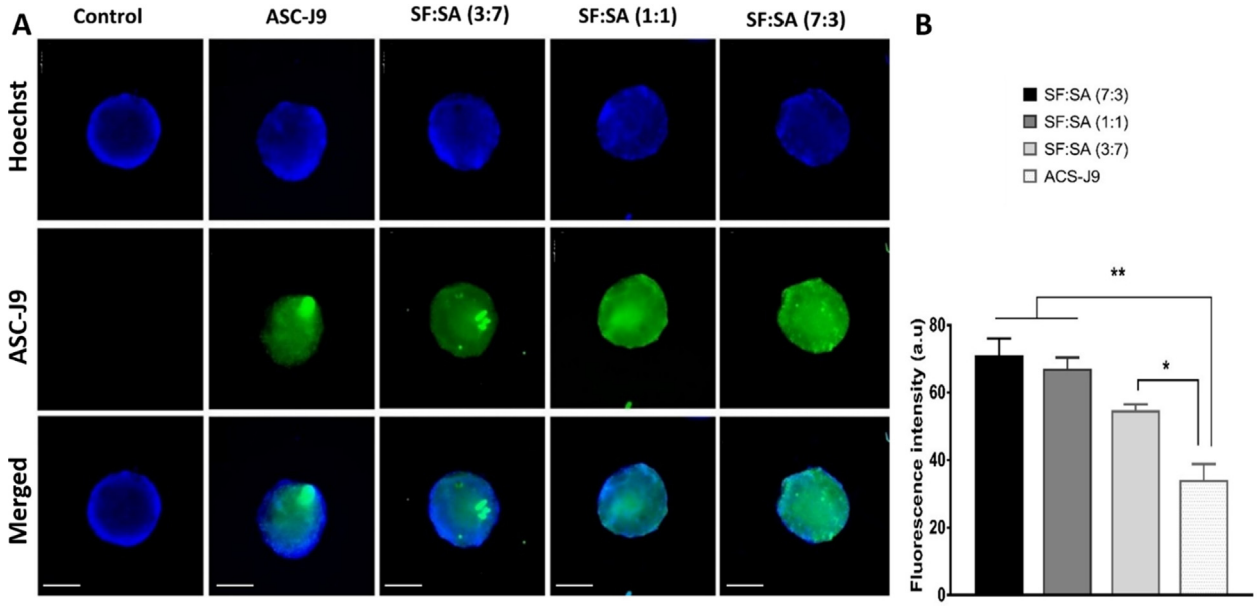

Fig. 6. (**A**) High content fluorescent microscope images showing uptake of ASC-J9 molecules and ASC-J9 loaded nanocarriers by HCT 116 tumour spheroids (×2 magnification, scale bars represent 400 μm). (**B**) The fluorescent intensity of ASC-J9 within the spheroids. An asterisk denotes statistical significance as follows: *P < 0.05, **P < 0.01.

than the 2D cell culture. [42,43]. Spheroids generated form HCT 116 cells (with a diameter of 600–800 μm) were used to assess the penetration and anticancer effect of the ASC-J9 loaded on the designed nanocarriers into the tumours. The tumour penetration study using the mean fluorescence intensity was previously reported [44]. As it could be clearly observed in Fig. 6.A, the drug fluorescence appears to be quite uniformly distributed across the spheroids. A drastic increase in the fluorescence intensity was detected in the spheroids treated with ASC-J9 loaded nanocarriers in comparison to the spheroids treated with the free drug. Furthermore, there was a significant difference in the fluorescence intensity of the drug within the spheroids treated with different nanocarrier formulations (Fig. 6.B). The SF:SA (7:3) formulation (with low stiffness) had the highest fluorescence intensity followed by SF:SA (1:1) and SF:SA (3:7) respectively. The observed difference in the drug penetration into tumour spheroids is attributed to the different elasticity of the nanocarrier formulations providing a tool for tuning the cellular uptake of the drug-loaded nanocarriers through changing the composition of the nanocarrier cores.

4. Conclusion

SF is a biocompatible biopolymer which has been approved by FDA for pharmaceutical applications. Therefore, it has gained great attention as the main ingredient in various drug delivery systems. Although the nature of SF protein is desirable, formulating SF as stable nanocarriers with controllable properties remains a challenge. Herein, we report the development of a very versatile, stable nanocarrier system using a blend of SF and SA in a lipid template for enhanced encapsulation and controlled release of the hydrophobic anticancer agent ASC-J9. The designed nanocarriers were prepared using a simple method that avoids harsh preparation conditions such as extreme heat, pH or organic solvents and enjoyed controllable size (using the extruded lipid template technique) and tunable stiffness (via changing the SF/SA ratio). The presented technique addresses the common limitations in formulating protein-based nanostructures such as lack of controllability of size and shape [15]. In addition, tuning the stiffness of the nanocarriers resulted in changes to the drug release and anticancer activity of the ASC-J9 in HCT 116 colorectal cancer cells. Our findings also display for the first time a significant increase in cellular uptake of ASC-J9 within its $t_{1/2}$ window when loaded into the nanocarrier systems and a prolonged anticancer activity resulting in the prevention of the colorectal cancer cell recovery in comparison to the free drug which may be of significance in preventing MDR. Modifying the nanocarrier properties also affected their penetration into the 3D tumour spheroids which serve as a model for solid tumours. Despite the large number of factors that govern the mechanism of cellular uptake in tumours, the results of this study suggest that tailoring the stiffness of the anticancer nanocarriers should be considered in the rational design of anticancer drug delivery systems.

CRediT authorship contribution statement

Mhd Anas Tomeh: Conceptualization, Methodology, Investigation, Validation, Formal analysis, Data curation, Visualization, Writing - original draft, Writing - review & editing. **Roja Hadianamrei:** Methodology, Writing - review & editing. **Weizhen Sun:** Methodology. **Defeng Xu:** Resources. **Stephen Brown:** Methodology, Supervision. **Xiubo Zhao:** Conceptualization, Methodology, Visualization, Writing - review & editing, Supervision, Project administration, Funding acquisition.

Declaration of Competing Interest

The authors declare that they have no known competing financial interests or personal relationships that could have appeared to influence the work reported in this paper.

Acknowledgement

The authors would like to thank EPSRC (EP/N007174/1 and EP/N023579/1), The Royal Society (RG160662), and Jiangsu specially appointed professor program for support. R.H. thanks the University of Sheffield for studentship. The authors also would like to thank the Nanocharacterization lab at Henry Royce Institute and TEM officer Mr Chris Hill for the technical support.

References

[1] D. Peer, J.M. Karp, S. Hong, O.C. Farokhzad, R. Margalit, R. Langer, Nanocarriers as an emerging platform for cancer therapy, Nat. Nanotechnol. 2 (2007) 751.
[2] P. Grodzinski, M. Kircher, M. Goldberg, A. Gabizon, Integrating Nanotechnology into Cancer Care, ACS Nano 13 (7) (2019) 7370–7376.
[3] M.A. Tomeh, X. Zhao, Recent Advances in Microfluidics for the Preparation of Drug and Gene Delivery Systems, Mol. Pharm. 17 (12) (2020) 4421–4434.
[4] V. Wagner, A. Dullaart, A.K. Bock, A. Zweck, The emerging nanomedicine landscape, Nat. Biotechnol. 24 (10) (2006) 1211–1217.
[5] R. Ravichandran, Nanoparticles in Drug Delivery: Potential Green Nanobiomedicine Applications, Int. J. Green Nanotechnol. Biomed. 1 (2) (2009) B108–B130.
[6] J. Xie, Z. Yang, C. Zhou, J. Zhu, R.J. Lee, L. Teng, Nanotechnology for the delivery of phytochemicals in cancer therapy, Biotechnol. Adv. 34 (4) (2016) 343–353.
[7] P. Ananthakrishnan, F.L. Balci, J.P. Crowe, Optimizing surgical margins in breast conservation, Int J Surg Oncol 2012 (2012) 585670.
[8] H. Wang, T. Vo, A. Hajar, S. Li, X. Chen, A.M. Parissenti, D.N. Brindley, Z. Wang, Multiple mechanisms underlying acquired resistance to taxanes in selected docetaxel-resistant MCF-7 breast cancer cells, BMC Cancer 14 (2014) 37.
[9] J. Chen, L. Lu, Y. Feng, H. Wang, L. Dai, Y. Li, P. Zhang, PKD2 mediates multi-drug resistance in breast cancer cells through modulation of P-glycoprotein expression, Cancer Lett. 300 (1) (2011) 48–56.
[10] X. Xue, X.-J. Liang, Overcoming drug efflux-based multidrug resistance in cancer with nanotechnology, Chin. J. Cancer 31 (2) (2012) 100–109.
[11] S.F. Soh, C.K. Huang, S.O. Lee, D. Xu, S. Yeh, J. Li, E.L. Yong, Y. Gong, C. Chang, Determination of androgen receptor degradation enhancer ASC-J9((R)) in mouse sera and organs with liquid chromatography tandem mass spectrometry, J. Pharm. Biomed. Anal. 88 (2014) 117–122.
[12] M.A. Cheng, F.-J. Chou, K. Wang, R. Yang, J. Ding, Q. Zhang, G. Li, S. Yeh, D. Xu, C. Chang, Androgen receptor (AR) degradation enhancer ASC-J9® in an FDA-approved formulated solution suppresses castration resistant prostate cancer cell growth, Cancer Lett. 417 (2018) 182–191.
[13] K. Dong, Z. Liu, Z. Li, J. Ren, X. Qu, Hydrophobic Anticancer Drug Delivery by a 980 nm Laser-Driven Photothermal Vehicle for Efficient Synergistic Therapy of Cancer Cells In Vivo, Adv. Mater. 25 (32) (2013) 4452–4458.
[14] P. Verderio, L. Pandolfi, S. Mazzucchelli, M.R. Marinozzi, R. Vanna, F. Gramatica, F. Corsi, M. Colombo, C. Morasso, D. Prosperi, Antiproliferative Effect of ASC-J9 Delivered by PLGA Nanoparticles against Estrogen-Dependent Breast Cancer Cells, Mol. Pharm. 11 (8) (2014) 2864–2875.
[15] W. Song, M. Muthana, J. Mukherjee, R.J. Falconer, C.A. Biggs, X. Zhao, Magnetic-Silk Core-Shell Nanoparticles as Potential Carriers for Targeted Delivery of Curcumin into Human Breast Cancer Cells, ACS Biomater. Sci. Eng. 3 (6) (2017) 1027–1038.
[16] F. Gentile, C. Chiappini, D. Fine, R.C. Bhavane, M.S. Peluccio, M.-M.-C. Cheng, X. Liu, M. Ferrari, P. Decuzzi, The effect of shape on the margination dynamics of non-neutrally buoyant particles in two-dimensional shear flows, J. Biomech. 41 (10) (2008) 2312–2318.
[17] Y. Geng, P. Dalhaimer, S. Cai, R. Tsai, M. Tewari, T. Minko, D.E. Discher, Shape effects of filaments versus spherical particles in flow and drug delivery, Nat. Nanotechnol. 2 (4) (2007) 249–255.
[18] Y. Yamamoto, Y. Nagasaki, Y. Kato, Y. Sugiyama, K. Kataoka, Long-circulating poly(ethylene glycol)-poly(D, L-lactide) block copolymer micelles with modulated surface charge, J. Control Release 77 (1–2) (2001) 27–38.
[19] Y. Li, K. Xiao, J. Luo, J. Lee, S. Pan, K.S. Lam, A novel size-tunable nanocarrier system for targeted anticancer drug delivery, J. Control Release 144 (3) (2010) 314–323.
[20] X. Banquy, F. Suarez, A. Argaw, J.-M. Rabanel, P. Grutter, J.-F. Bouchard, P. Hildgen, S. Giasson, Effect of mechanical properties of hydrogel nanoparticles on macrophage cell uptake, Soft Matter 5 (20) (2009) 3984–3991.
[21] V.P. Torchilin, Recent advances with liposomes as pharmaceutical carriers, Nat. Rev. Drug Discovery 4 (2005) 145.
[22] P. Pradhan, J. Giri, F. Rieken, C. Koch, O. Mykhaylyk, M. Doblinger, R. Banerjee, D. Bahadur, C. Plank, Targeted temperature sensitive magnetic liposomes for thermo-chemotherapy, J. Control Release 142 (1) (2010) 108–121.
[23] T. Wongpinyochit, P. Uhlmann, A.J. Urquhart, F.P. Seib, PEGylated Silk Nanoparticles for Anticancer Drug Delivery, Biomacromolecules 16 (11) (2015) 3712–3722.
[24] S. Wilhelm, A.J. Tavares, Q. Dai, S. Ohta, J. Audet, H.F. Dvorak, W.C.W. Chan, Analysis of nanoparticle delivery to tumours, Nat. Rev. Mater. 1 (2016) 16014.
[25] D. Sutton, N. Nasongkla, E. Blanco, J. Gao, Functionalized micellar systems for cancer targeted drug delivery, Pharm. Res. 24 (6) (2007) 1029–1046.
[26] J. Liu, H. Lee, C. Allen, Formulation of drugs in block copolymer micelles: drug loading and release, Curr. Pharm. Des. 12 (36) (2006) 4685–4701.
[27] Y.-J. Lu, E.-Y. Chuang, Y.-H. Cheng, T.S. Anilkumar, H.-A. Chen, J.-P. Chen, Thermosensitive magnetic liposomes for alternating magnetic field-inducible drug delivery in dual targeted brain tumor chemotherapy, Chem. Eng. J. 373 (2019) 720–733.
[28] M.A. Tomeh, R. Hadianamrei, X. Zhao, Silk Fibroin as a Functional Biomaterial for Drug and Gene Delivery, Pharmaceutics 11 (10) (2019) 494.
[29] S. Hofmann, C.T. Foo, F. Rossetti, M. Textor, G. Vunjak-Novakovic, D.L. Kaplan, H.P. Merkle, L. Meinel, Silk fibroin as an organic polymer for controlled drug delivery, J. Control Release 111 (1–2) (2006) 219–227.
[30] A.B. Li, J.A. Kluge, N.A. Guziewicz, F.G. Omenetto, D.L. Kaplan, Silk-based stabilization of biomacromolecules, J. Control. Release 219 (2015) 416–430.
[31] M. Choi, D. Choi, J. Hong, Multilayered Controlled Drug Release Silk Fibroin Nanofilm by Manipulating Secondary Structure, Biomacromolecules 19 (7) (2018) 3096–3103.
[32] C. Vepari, D.L. Kaplan, Silk as a Biomaterial, Prog. Polym. Sci. 32 (8–9) (2007) 991–1007.
[33] M.A. de Moraes, M.F. Silva, R.F. Weska, M.M. Beppu, Silk fibroin and sodium alginate blend: Miscibility and physical characteristics, Mater. Sci. Eng., C 40 (2014) 85–91.
[34] Q. Ma, J. Cao, Y. Gao, S. Han, Y. Liang, T. Zhang, X. Wang, Y. Sun, Microfluidic-mediated nano-drug delivery systems: from fundamentals to fabrication for advanced therapeutic applications, Nanoscale 12 (29) (2020) 15512–15527.
[35] P. Guo, D. Liu, K. Subramanyam, B. Wang, J. Yang, J. Huang, D.T. Auguste, M.A. Moses, Nanoparticle elasticity directs tumor uptake, Nat. Commun. 9 (1) (2018) 130.
[36] J. Sun, L. Zhang, J. Wang, Q. Feng, D. Liu, Q. Yin, D. Xu, Y. Wei, B. Ding, X. Shi, X. Jiang, Tunable Rigidity of (Polymeric Core)–(Lipid Shell) Nanoparticles for Regulated Cellular Uptake, Adv. Mater. 27 (8) (2015) 1402–1407.
[37] W. Zhang, B. Han, X. Lai, C. Xiao, S. Xu, X. Meng, Z. Li, J. Meng, T. Wen, X. Yang, J. Liu, H. Xu, Stiffness of cationized gelatin nanoparticles is a key factor determining RNAi efficiency in myeloid leukemia cells, Chem. Commun. 56 (8) (2020) 1255–1258.
[38] J.I. Solomun, J.D. Totten, T. Wongpinyochit, A.J. Florence, F.P. Seib, Manual Versus Microfluidic-Assisted Nanoparticle Manufacture: Impact of Silk Fibroin Stock on Nanoparticle Characteristics, ACS Biomater. Sci. Eng. 6 (5) (2020) 2796–2804.
[39] M. Yu, L. Xu, F. Tian, Q. Su, N. Zheng, Y. Yang, J. Wang, A. Wang, C. Zhu, S. Guo, X. Zhang, Y. Gan, X. Shi, H. Gao, Rapid transport of deformation-tuned nanoparticles across biological hydrogels and cellular barriers, Nat. Commun. 9 (1) (2018) 2607.
[40] M. Szekalska, A. Puciłowska, E. Szymańska, P. Ciosek, K. Winnicka, Alginate: current use and future perspectives in pharmaceutical and biomedical applications, Int. J. Polym. Sci. 2016 (2016) 7697031.
[41] B.F. Mogharbel, J.C. Francisco, A.C. Irioda, D.S.M. Dziedzic, P.E. Ferreira, D. de Souza, C.M.C.O. de Souza, N.B. Neto, L.C. Guarita-Souza, C.R.C. Franco, C.V. Nakamura, V. Kaplum, L. Mazzarino, E. Lemos-Senna, R. Borsali, P.A. Soto, P. Setton-Avruj, E. Abdelwahid, K.A.T. de Carvalho, Fluorescence properties of curcumin-loaded nanoparticles for cell tracking, Int. J. Nanomed. 13 (2018) 5823–5836.
[42] M. Zanoni, F. Piccinini, C. Arienti, A. Zamagni, S. Santi, R. Polico, A. Bevilacqua, A. Tesei, 3D tumor spheroid models for in vitro therapeutic screening: a systematic approach to enhance the biological relevance of data obtained, Sci. Rep. 6 (1) (2016) 19103.
[43] E. Fennema, N. Rivron, J. Rouwkema, C. van Blitterswijk, J. de Boer, Spheroid culture as a tool for creating 3D complex tissues, Trends Biotechnol. 31 (2) (2013) 108–115.
[44] M.K. Riaz, X. Zhang, K.H. Wong, H. Chen, Q. Liu, X. Chen, G. Zhang, A. Lu, Z. Yang, Pulmonary delivery of transferrin receptors targeting peptide surface-functionalized liposomes augments the chemotherapeutic effect of quercetin in lung cancer therapy, Int. J. Nanomed. 14 (2019) 2879–2902.